Appl. Phys. B (2012) 109:649–658
DOI 10.1007/s00340-012-5233-0

Applied Physics B
Lasers and Optics

Crystal-host $Gd_{0.5}Lu_{0.5}VO_4$ for Ln^{3+}-lasants: a new high-gain many-phonon $\chi^{(3)}$-active tetragonal vanadate—SRS spectroscopy and nonlinear-laser effects

On the 50th anniversary of the discovery of stimulated Raman scattering

A. A. Kaminskii · O. Lux · H. Rhee · H. J. Eichler · H. Yoneda · A. Shirakawa · K. Ueda · B. Zhao · J. Chen · J. Dong · J. Zhang

Received: 16 May 2012 / Revised: 27 July 2012 / Published online: 16 October 2012

Abstract We found that tetragonal $Gd_{0.5}Lu_{0.5}VO_4$—known as host-crystal for Ln^{3+}-lasants—is an attractive optical material for Raman laser converters. We discovered and investigated its almost sesqui-octave Stokes and anti-Stokes lasing comb resulting from four SRS-promoting vibration modes in combination with cascaded and cross-cascaded many-phonon $\chi^{(3)}$-nonlinear interactions. Furthermore, estimations of the steady-state Raman gain coefficient have been performed.

A. A. Kaminskii (✉)
Institute of Crystallography, Russian Academy of Sciences, Moscow 119333, Russia
e-mail: kaminalex@mail.ru

O. Lux · H. Rhee · H. J. Eichler
Institute of Optics and Atomic Physics, TU Berlin, 10623 Berlin, Germany
e-mail: oliver.lux@physik.tu-berlin.de

H. Yoneda · A. Shirakawa · K. Ueda
Institute for Laser Science, University of Electro-Communications, Tokyo 182-8585, Japan

B. Zhao · J. Chen
College of Chemistry and Chemical Engineering, Fuzhou University, Fuzhou 350108, China

J. Dong
Department of Electronic Engineering, School of Information and Technology of Xiamen University, Xiamen 361005, China

J. Zhang
Jiangsu Normal University, Xuzhou 221116, China

J. Zhang
Nanyang Technological University, Singapore 639798, Singapore

1 Introduction

Single crystals of rare-earth vanadates $REVO_4$ (RE = Y and lanthanides (Ln), except for La) with D_{4h}^{19}-tetragonal zircon-type structure ($ZrSiO_4$) receive high attention in modern laser and solid-state physics as well as in (nonlinear) optics (see e.g., [1, 2]). Since the mid-1960s, they are widely used as host-crystals for Ln^{3+}-lasants, especially for Nd^{3+} (see e.g., first publications [3–5]) and as optical materials with high birefringence [6].

One decade ago, efficient stimulated Raman scattering (SRS) was discovered in these vanadates which gave them new experimental lasing potential [7]. Having an unique combination of these properties, the $REVO_4$ vanadates have enriched the arsenal of practical crystalline materials used for modern laser technologies. Many-phonon SRS occurring in these crystals distinguishes them as attractive objects for solid-state physics and spectroscopy with respect to studies of the various manifestations of $\chi^{(3)}$-nonlinear photon–phonon interactions.

In recent years, also solid-solutions ("mixed" crystals) of the $REVO_4$:Ln^{3+} crystals have been investigated in order to realize a better adaption of the absorption and luminescence spectral properties to the radiative parameters of pumping semiconductor laser diodes. In case of solid-solutions, the RE-crystallographic D_{2d}-positions are statistically filled with two different RE^{3+}-ions (e.g., Y^{3+} and Gd^{3+} or Gd^{3+} and Lu^{3+}).

Typically, the desired effect is achieved when the two different RE^{3+}-ions fill the D_{2d}-positions in relation 1:1. In this case, the effective crystal field at the Ln^{3+}-lasants shows a maximum disorder which manifests itself in a small inhomogeneous broadening of their absorption and luminescence lines. Such crystals are partially disordered laser crystals in the classification of one of us (A.A.K., see e.g., [8,

9]) when it holds the second law (structural static) of crystal-field disorder at Ln^{3+}-lasants. It is now known for a sufficient number of laser crystals and crystalline ceramics (mainly oxide) of this class with varying degrees of crystal-field disorder at their Ln^{3+}-lasant ions (see review paper [2]). For "mixed" $REVO_4$:Ln^{3+} vanadates, the disordering is not so large. Therefore, the quasi-center concept of the Ln^{3+}-lasants can be applied within the framework of their spectroscopic analysis [8, 10]. Some selected data showing laser and nonlinear laser properties of the known usual (with single-type of Ln^{3+}-cations) and "mixed" (with two different types of Ln^{3+}-cations) vanadates are given in Table 2.

This article focuses on SRS spectroscopy of tetragonal $Gd_{0.5}Lu_{0.5}VO_4$ which exhibits a partially disordered crystal structure. It is performed within the series of our previous investigations of rare-earth vanadate crystals with tetragonal zircon-type structure ($TRVO_4$-type crystals) to identify their SRS-promoting vibration modes and to study the different manifestations of their $\chi^{(3)}$-nonlinear laser interactions.

2 Experimental setup

The spectroscopic analysis of room-temperature SRS lasing and $\chi^{(3)}$-nonlinear photon–phonon interactions in $Gd_{0.5}Lu_{0.5}VO_4$ was performed in single-pass (cavity-free) excitation scheme using a hybrid mode-locked Xe-flash lamp-pumped Nd^{3+}:$Y_3Al_5O_{12}$ picosecond laser as pump source. The emission wavelength of λ_{f1}= 1.06415 μm corresponds to the main laser inter-Stark transition $^4F_{3/2}\rightarrow{}^4I_{11/2}$ of the Nd^{3+}-ions [8, 24].

This non-commercial system is configured as a master oscillator power amplifier (MOPA) arrangement and operates at 1 Hz repetition rate. Cavity-dumping of the oscillator employing an intra-cavity Pockels cell generates single pulses with 80 ps duration while the subsequent double-pass amplifier increases the pulse energy to 40 mJ in order to provide the intensities needed to efficiently excite nonlinear processes in the investigated sample. The amplified beam is directed to the measuring part of the setup which is depicted in Fig. 1a.

An attenuator consisting of a revolving half-wave-plate ("$\lambda/2$") and a Glan-laser polarizer (P) allows for continuous variation of the pump pulse energy which is monitored by measuring a small portion of the radiation with a pyroelectric energy meter (Polytec RjP-735). A spherical, plano-convex lens (L_1) with a focal length of 250 mm is used to focus the nearly Gaussian pump beam into the $Gd_{0.5}Lu_{0.5}VO_4$ crystal, resulting in a beam waist diameter of about 80 μm.

Table 1 Some $\chi^{(3)}$-nonlinear laser data of SRS-active rare-earth vanadate crystals with tetragonal zircon-type structure

Crystal	Ln^{3+}-lasant ions	SRS-promoting vibration modes (cm^{-1})[a]	Manifestations of $\chi^{(3)}$-nonlinear interaction[a]	Self-Raman lasers[b]
YVO_4	Nd^{3+}, Ho^{3+} Er^{3+} Tm^{3+}, Yb^{3+}	≈890, ≈838, ≈815 [7, 11]	SRS, self-SFG(SRS)[c], THG(SRS)[d], $\chi^{(3)}$-cr-casc[e], $\chi^{(3)}$-comb[f]	Nd^{3+} ($^4F_{3/2}\rightarrow{}^4I_{11/2}$ [12], $^4F_{3/2}\rightarrow{}^4I_{13/2}$ [13]); Yb^{3+} ($^2F_{5/2}\rightarrow{}^2I_{7/2}$ [14])
$GdVO_4$	Nd^{3+}, Ho^{3+}, Er^{3+}, Tm^{3+}, Yb^{3+}	≈882, ≈807, ≈256 [7, 11]	SRS, self-SFG(SRS), THG(SRS), $\chi^{(3)}$-cr-casc, $\chi^{(3)}$-comb	Nd^{3+} ($^4F_{3/2}\rightarrow{}^4I_{11/2}$ [15], $^4F_{3/2}\rightarrow{}^4I_{13/2}$ [16])
$YbVO_4$		≈897, ≈823 [17]	SRS, self-SFG(SRS), THG(SRS), $\chi^{(3)}$-comb	
$LuVO_4$	Nd^{3+}, Tm^{3+}, Yb^{3+}	≈900, ≈826, ≈261, ≈113 [18]	SRS, self-SFG(SRS), THG, $\chi^{(3)}$-cr-casc, $\chi^{(3)}$-comb	Nd^{3+} ($^4F_{3/2}\rightarrow{}^4I_{11/2}$ [19])
$Y_{0.4}Gd_{0.6}VO_4$	Nd^{3+}, Yb^{3+}	≈882 [20] [g]	SRS	Nd^{3+} ($^4F_{3/2}\rightarrow{}^4I_{11/2}$ [20])
$Gd_{0.5}Lu_{0.5}VO_4$	Nd^{3+}	≈890, ≈813, ≈485, ≈260	**SRS, self-SFG(SRS), THG** $\chi^{(3)}$-cr-casc, $\chi^{(3)}$-comb	

[a] The results of this work are given in the bold letters

[b] Only pioneering publications are listed here. In recent years, many types of self-Raman lasers have been developed on the basis of $REVO_4$ crystals doped with Nd^{3+} and Yb^{3+} ions (see e.g., [21–24] and their references)

[c] Self-SFG(SRS): the sum-frequency generation arising from SRS lasing Stokes (anti-Stokes) components and the pumping radiation

[d] THG(SRS): the third harmonic generation by the parametric four-wave mixing (generation) with the participation of the pumping radiation at the fundamental wavelength (1.06415 μm) and its arising Stokes and anti-Stokes components

[e] $\chi^{(3)}$-cr-casc: the cascade of one or many step $\chi^{(3)}$-lasing when in the photon–phonon generation of high-order Stokes and anti-Stokes components involves the interaction of different SRS-active promoting vibrational modes of the crystal

[f] $\chi^{(3)}$-comb: the representation of the spectrum of Stokes and anti-Stokes laser frequency components with a width of at least one octave (the highest frequency (energy) component must be at least double the lowest frequency component

[g] The data on the SRS-active vibrational mode of this crystal should be clarified

Table 2 Spectral composition of high-order many-phonon cascaded and cross-cascaded Raman-induced Stokes and anti-Stokes $\chi^{(3)}$-nonlinear generation of tetragonal $Gd_{0.5}Lu_{0.5}VO_4$, recorded at room temperature with a picosecond Nd^{3+}:$Y_3Al_5O_{12}$ laser operating at the two fundamental wavelengths $\lambda_{f1} = 1.06415$ μm and $\lambda_{f2} = 0.53207$ μm (SHG)

Excitation condition		Nonlinear $\chi^{(3)}$- lasing components			SRS-promoting vibration modes, cm^{-1}			
λ_f, μm	Pumping condition[a]	Wavelength, μm[b]	Line[c]	Attribution of nonlinear generation[d]	ω_{SRS1}	ω_{SRS2}	ω_{SRS3}	ω_{SRS4}
1.06415	*c*(*a*, *a*)*c*	0.8947	$ASt_{2\text{-}1}$	$*\omega_{f1} + 2\omega_{SRS1} = \omega_{ASt2\text{-}1}$	≈890			
	(see Fig. 2)	0.9253	$ASt_{1\text{-}3}ASt_{1\text{-}1}$	$**\omega_{f1} + \omega_{SRS1} + 2\omega_{SRS3} = \omega_{ASt2\text{-}3,ASt1\text{-}1}$	≈890		≈260	
		0.9481	$ASt_{2\text{-}3}ASt_{1\text{-}1}$	$**\omega_{f1} + \omega_{SRS1} + \omega_{SRS3} = \omega_{ASt1\text{-}3,ASt1\text{-}1}$	≈890		≈260	
		0.9721	$ASt_{1\text{-}1}$	$*\omega_{f1} + \omega_{SRS1} = \omega_{ASt1\text{-}1}$	≈890			
		0.9973	$St_{1\text{-}3}ASt_{1\text{-}1}$	$**\omega_{f1} + \omega_{SRS1} - \omega_{SRS3} = \omega_{St1\text{-}3,ASt1\text{-}1}$	≈890		≈260	
		1.0238	$St_{2\text{-}3}ASt_{1\text{-}1}$	$**\omega_{f1} + \omega_{SRS1} - 2\omega_{SRS3} = \omega_{ASt2\text{-}3,ASt1\text{-}1}$	≈890		≈260	
		1.0355	$ASt_{1\text{-}3}$	$*\omega_{f1} + \omega_{SRS3} = \omega_{ASt1\text{-}3}$			≈260	
		1.06415	λ_{f1}	ω_{f1}				
		1.0944	$St_{1\text{-}3}$	$\omega_{f1} - \omega_{SRS3} = \omega_{St1\text{-}3}$			≈260	
		1.1265	$St_{2\text{-}3}$	$*\omega_{f1} - 2\omega_{SRS3} = \omega_{St2\text{-}3}$			≈260	
		1.1755	$St_{1\text{-}1}$	$\omega_{f1} - \omega_{SRS1} = \omega_{St1\text{-}1}$	≈890			
	c(*ab*, *ab*)*c*	0.8886	$St_{1\text{-}2}ASt_{3\text{-}1}$	$**\omega_{f1} + 3\omega_{SRS1} - \omega_{SRS2} = \omega_{St1\text{-}2,ASt3\text{-}1}$	≈890	≈813		
	(see Fig. 3)	0.8947	$ASt_{2\text{-}1}$	$*\omega_{f1} + 2\omega_{SRS1} = \omega_{ASt2\text{-}1}$	≈890			
		0.9009	$ASt_{1\text{-}2}ASt_{1\text{-}1}$	$**\omega_{f1} + \omega_{SRS1} + \omega_{SRS2} = \omega_{ASt1\text{-}2,ASt1\text{-}1}$	≈890	≈813		
		0.9072	$ASt_{2\text{-}2}$	$*\omega_{f1} + 2\omega_{SRS2} = \omega_{ASt2\text{-}2}$		≈813		
		0.9160	$St_{1\text{-}3}ASt_{2\text{-}1}$	$**\omega_{f1} + 2\omega_{SRS1} - \omega_{SRS3} = \omega_{St1\text{-}3,ASt2\text{-}1}$	≈890	≈813		
		0.9217	$ASt_{1\text{-}4}St_{1\text{-}2}ASt_{2\text{-}1}$	$**\omega_{f1} + 2\omega_{SRS1} - \omega_{SRS2} + \omega_{SRS4} = \omega_{ASt1\text{-}4,St1\text{-}2,ASt2\text{-}1}$	≈890		≈260	
		0.9286	$St_{1\text{-}4}St_{1\text{-}2}ASt_{3\text{-}1}$	$**\omega_{f1} + 3\omega_{SRS1} - \omega_{SRS2} - \omega_{SRS4} = \omega_{St1\text{-}4,St1\text{-}2,ASt3\text{-}1}$	≈890	≈813		≈485
		0.9481	$ASt_{1\text{-}3}ASt_{1\text{-}1}$	$**\omega_{f1} + \omega_{SRS1} + \omega_{SRS3} = \omega_{ASt1\text{-}3,ASt1\text{-}1}$	≈890		≈260	
		0.9649	$St_{1\text{-}2}ASt_{2\text{-}1}$	$**\omega_{f1} + 2\omega_{SRS1} - \omega_{SRS2} = \omega_{At1\text{-}2,ASt2\text{-}1}$	≈890	≈813		
		0.9721	$ASt_{1\text{-}1}$	$*\omega_{f1} + \omega_{SRS1} = \omega_{ASt1\text{-}1}$	≈890			
		0.9794	$ASt_{1\text{-}2}$	$*\omega_{f1} + \omega_{SRS2} = \omega_{ASt1\text{-}2}$		≈813		
		0.9869	$ASt_{2\text{-}2}St_{1\text{-}1}$	$**\omega_{f1} - \omega_{SRS1} + \omega_{SRS2} = \omega_{ASt2\text{-}2,St1\text{-}1}$	≈890	≈813		
		0.9973	$St_{1\text{-}3}ASt_{1\text{-}1}$	$**\omega_{f1} + \omega_{SRS1} - \omega_{SRS3} = \omega_{St1\text{-}3,ASt1\text{-}1}$	≈890		≈260	
		1.0041	$ASt_{1\text{-}3}ASt_{1\text{-}1}$	$**\omega_{f1} + \omega_{SRS1} + \omega_{SRS3} = \omega_{ASt1\text{-}3,ASt1\text{-}1}$	≈890		≈260	
		1.0238	$ASt_{1\text{-}4}St_{1\text{-}2}ASt_{1\text{-}1}$	$**\omega_{f1} + \omega_{SRS1} - \omega_{SRS2} + \omega_{SRS4} = \omega_{ASt1\text{-}4,St1\text{-}2,ASt1\text{-}1}$	≈890	≈813		≈485
		1.0355	$ASt_{1\text{-}3}$	$*\omega_{f1} + \omega_{SRS3} = \omega_{ASt1\text{-}3}$			≈260	
		1.0470	$St_{2\text{-}2}ASt_{2\text{-}1}$	$**\omega_{f1} + 2\omega_{SRS1} - 2\omega_{SRS2} = \omega_{St2\text{-}2,ASt2\text{-}1}$	≈890	≈813		
		1.0555	$St_{1\text{-}2}ASt_{1\text{-}1}$	$**\omega_{f1} + \omega_{SRS1} - \omega_{SRS2} = \omega_{St1\text{-}2,ASt1\text{-}1}$	≈890	≈813		
		1.06415	λ_{f1}	ω_{f1}				
		1.0730	$ASt_{1\text{-}2}St_{1\text{-}1}$	$**\omega_{f1} - \omega_{SRS1} + \omega_{SRS2} = \omega_{ASt1\text{-}2,St1\text{-}1}$	≈890	≈813		
		1.0819	$ASt_{2\text{-}2}St_{2\text{-}1}$	$**\omega_{f1} - 2\omega_{SRS1} + 2\omega_{SRS2} = \omega_{ASt2\text{-}2,St2\text{-}1}$	≈890	≈813		
		1.0944	$St_{1\text{-}3}$	$\omega_{f1} - \omega_{SRS3} = \omega_{St1\text{-}3}$			≈260	

Table 2 continued

Excitation condition		Nonlinear $\chi^{(3)}$- lasing components			SRS-promoting vibration modes, cm^{-1}			
λ_f, μm	Pumping condition[a]	Wavelength, μm[b]	Line[c]	Attribution of nonlinear generation[d]	ω_{SRS1}	ω_{SRS2}	ω_{SRS3}	ω_{SRS4}
		1.1319	$St_{1-4}ASt_{1-2}St_{1-1}$	$^{**}\omega_{f1} - \omega_{SRS1} + \omega_{SRS2} - \omega_{SRS4} = \omega_{St1-4,ASt1-2,St1-1}$	≈890	≈813		≈485
		1.1406	$ASt_{1-3}St_{1-1}$	$^{**}\omega_{f1} - \omega_{SRS1} + \omega_{SRS3} = \omega_{ASt1-3,St1-1}$	≈890		≈260	
		1.1649	St_{1-2}	$\omega_{f1} - \omega_{SRS2} = \omega_{St1-2}$		≈813		
		1.1755	St_{1-1}	$\omega_{f1} - \omega_{SRS1} = \omega_{St1-1}$	≈890			
		1.1862	$ASt_{1-2}St_{2-1}$	$^{**}\omega_{f1} - 2\omega_{SRS1} + \omega_{SRS2} = \omega_{ASt1-2,St2-1}$	≈890	≈813		
1.06415	*c*(*ab*, *ab*)*c*	0.5745	ASt_{9-1}	$^{*}\omega_{f1} + 9\omega_{SRS1} = \omega_{ASt9-1}$	≈890			
	(see Fig. 4)	0.6054	ASt_{8-1}	$^{*}\omega_{f1} + 8\omega_{SRS1} = \omega_{ASt8-1}$	≈890			
		0.6399	ASt_{7-1}	$^{*}\omega_{f1} + 7\omega_{SRS1} = \omega_{ASt7-1}$	≈890			
		0.6507	$St_{1-3}ASt_{7-1}$	$^{**}\omega_{f1} + 7\omega_{SRS1} - \omega_{SRS3} = \omega_{St1-3,ASt7-1}$	≈890		≈260	
		0.6668	$ASt_{1-3}ASt_{6-1}$	$^{**}\omega_{f1} + 6\omega_{SRS1} + \omega_{SRS3} = \omega_{ASt1-3,ASt6-1}$	≈890		≈260	
		0.6786	ASt_{6-1}	$^{*}\omega_{f1} + 6\omega_{SRS1} = \omega_{ASt6-1}$	≈890			
		0.6907	$St_{1-3}ASt_{6-1}$	$^{**}\omega_{f1} + 6\omega_{SRS1} - \omega_{SRS3} = \omega_{St1-3,ASt6-1}$	≈890		≈260	
		0.7089	$ASt_{1-3}ASt_{5-1}$	$^{**}\omega_{f1} + 5\omega_{SRS1} + \omega_{SRS3} = \omega_{ASt1-3,ASt5-1}$	≈890		≈260	
		0.7222	ASt_{5-1}	$^{*}\omega_{f1} + 5\omega_{SRS1} = \omega_{ASt5-1}$	≈890			
		0.7360	$St_{1-3}ASt_{5-1}$	$^{**}\omega_{f1} + 5\omega_{SRS1} - \omega_{SRS3} = \omega_{St1-3,ASt5-1}$	≈890		≈260	
		0.7566	$ASt_{1-3}ASt_{4-1}$	$^{**}\omega_{f1} + 4\omega_{SRS1} + \omega_{SRS3} = \omega_{ASt1-3,ASt4-1}$	≈890		≈260	
		0.7718	ASt_{4-1}	$^{*}\omega_{f1} + 4\omega_{SRS1} = \omega_{ASt4-1}$	≈890			
		0.7876	$St_{1-3}ASt_{4-1}$	$^{**}\omega_{f1} + 4\omega_{SRS1} - \omega_{SRS3} = \omega_{St1-3,ASt4-1}$	≈890		≈260	
		0.8112	$ASt_{1-3}ASt_{3-1}$	$^{**}\omega_{f1} + 3\omega_{SRS1} + \omega_{SRS3} = \omega_{ASt1-3,ASt3-1}$	≈890		≈260	
		0.8287	ASt_{3-1}	$^{*}\omega_{f1} + 3\omega_{SRS1} = \omega_{ASt3-1}$	≈890			
		0.8340	$ASt_{1-2}ASt_{2-1}$	$^{**}\omega_{f1} + 2\omega_{SRS1} + \omega_{SRS2} = \omega_{ASt1-2,ASt2-1}$	≈890	≈813		
		0.8469	$St_{1-3}ASt_{3-1}$	$^{**}\omega_{f1} + 3\omega_{SRS1} - \omega_{SRS3} = \omega_{St1-3,ASt3-1}$	≈890		≈260	
		0.8743	$ASt_{1-3}ASt_{2-1}$	$^{**}\omega_{f1} + 2\omega_{SRS1} + \omega_{SRS3} = \omega_{ASt1-3,ASt2-1}$	≈890		≈260	
		0.8947	ASt_{2-1}	$^{*}\omega_{f1} + 2\omega_{SRS1} = \omega_{ASt2-1}$	≈890			
		0.9009	$ASt_{1-2}ASt_{1-1}$	$^{**}\omega_{f1} + \omega_{SRS1} + \omega_{SRS2} = \omega_{ASt1-2,ASt1-1}$	≈890	≈813		
		0.9160	$St_{1-3}ASt_{2-1}$	$^{**}\omega_{f1} + 2\omega_{SRS1} - \omega_{SRS3} = \omega_{St1-3,ASt2-1}$	≈890		≈260	
		0.9217	$ASt_{1-4}St_{1-2}ASt_{2-1}$	$^{**}\omega_{f1} + 2\omega_{SRS1} - \omega_{SRS2} + \omega_{SRS4} = \omega_{ASt1-4,St1-2,ASt2-1}$	≈890	≈813		≈485
		0.9350	$ASt_{1-4}ASt_{1-2}$	$^{**}\omega_{f1} + \omega_{SRS2} + \omega_{SRS4} = \omega_{ASt1-4,ASt1-2}$		≈813		≈485
		0.9481	$ASt_{1-3}ASt_{1-1}$	$^{**}\omega_{f1} + \omega_{SRS1} + \omega_{SRS3} = \omega_{ASt1-3,ASt1-1}$	≈890		≈260	
		0.9649	$St_{1-2}ASt_{2-1}$	$^{**}\omega_{f1} + 2\omega_{SRS1} - \omega_{SRS2} = \omega_{St1-2,ASt2-1}$	≈890	≈813		
		0.9721	ASt_{1-1}	$^{*}\omega_{f1} + \omega_{SRS1} = \omega_{ASt1-1}$	≈890			
		0.9794	ASt_{1-2}	$^{*}\omega_{f1} + \omega_{SRS2} = \omega_{ASt1-2}$		≈813		
		0.9973	$St_{1-3}ASt_{1-1}$	$^{**}\omega_{f1} + \omega_{SRS1} - \omega_{SRS3} =$	≈890		≈260	

Table 2 continued

Excitation condition		Nonlinear $\chi^{(3)}$- lasing components			SRS-promoting vibration modes, cm^{-1}			
λ_f, μm	Pumping condition[a]	Wavelength, μm[b]	Line[c]	Attribution of nonlinear generation[d]	ω_{SRS1}	ω_{SRS2}	ω_{SRS3}	ω_{SRS4}
		1.0041	$ASt_{1-4}St_{1-2}ASt_{1-1}$	$\omega_{St1-3,ASt1-1}$ **$\omega_{f1} + \omega_{SRS1} - \omega_{SRS2}+ \omega_{SRS4} = \omega_{ASt1-4,St1-2,ASt1-1}$	≈890	≈813		≈485
		1.0283	$St_{1-4}ASt_{1-2}$	**$\omega_{f1} + \omega_{SRS2} - \omega_{SRS4} = \omega_{St1-4,ASt1-2}$		≈813		≈485
		1.0355	ASt_{1-3}	*$\omega_{f1} + \omega_{SRS3} = \omega_{ASt1-3}$			≈260	
		1.0555	$St_{1-2}ASt_{1-1}$	**$\omega_{f1} + \omega_{SRS1} - \omega_{SRS2} = \omega_{St1-2,ASt1-1}$	≈890	≈813		
		1.06415	λ_{f1}	ω_{f1}				
	c(*ab*, *ab*)*c*	1.0355	ASt_{1-3}	*$\omega_{f1} + \omega_{SRS3} = \omega_{ASt1-3}$			≈260	
	(see Fig. 5)	1.0555	$St_{1-2}ASt_{1-1}$	**$\omega_{f1} + \omega_{SRS1} - \omega_{SRS2} = \omega_{St1-2,ASt1-1}$	≈890	≈813		
		1.06415	λ_{f1}	ω_{f1}				
		1.0730	$ASt_{1-2}St_{1-1}$	**$\omega_{f1} - \omega_{SRS1} + \omega_{SRS2} = \omega_{ASt1-2,St1-1}$	≈890	≈813		
		1.0944	St_{1-3}	$\omega_{f1} - \omega_{SRS3} = \omega_{St1-3}$			≈260	
		1.1265	St_{2-3}	*$\omega_{f1} - 2\omega_{SRS3} = \omega_{St2-3}$			≈260	
		1.1307	$ASt_{1-3}St_{1-2}$	**$\omega_{f1} - \omega_{SRS2} + \omega_{SRS3} = \omega_{ASt1-3,St1-2}$		≈813	≈260	
1.06415	*c*(*ab*, *ab*)*c*	1.1406	$ASt_{1-3}St_{1-1}$	**$\omega_{f1} - \omega_{SRS1} + \omega_{SRS3} = \omega_{ASt1-3,St1-1}$	≈890		≈260	
	(see Fig. 5)	1.1546	$St_{2-2}ASt_{1-1}$	**$\omega_{f1} + \omega_{SRS1} - 2\omega_{SRS2} = \omega_{St2-2,ASt1-1}$	≈890	≈813		
		1.1649	St_{1-2}	$\omega_{f1} - \omega_{SRS2} = \omega_{St1-2}$		≈813		
		1.1755	St_{1-1}	$\omega_{f1} - \omega_{SRS1} = \omega_{St1-1}$	≈890			
		1.1862	$ASt_{1-2}St_{2-1}$	**$\omega_{f1} - 2\omega_{SRS1} + \omega_{SRS2} = \omega_{ASt1-2,St2-1}$	≈890	≈813		
		1.2013	$St_{1-3}St_{1-2}$	**$\omega_{f1} - \omega_{SRS2} - \omega_{SRS3} = \omega_{St1-3,St1-2}$		≈813	≈260	
		1.2125	$St_{1-3}St_{1-1}$	**$\omega_{f1} - \omega_{SRS1} - \omega_{SRS3} = \omega_{St1-3,St1-1}$	≈890		≈260	
		1.2520	$St_{2-3}St_{1-1}$	**$\omega_{f1} - \omega_{SRS1} - 2\omega_{SRS3} = \omega_{St2-3,St1-1}$	≈890		≈260	
		1.2572	$ASt_{1-3}St_{1-2}St_{1-1}$	**$\omega_{f1} - \omega_{SRS1} - \omega_{SRS2}+ \omega_{SRS3} = \omega_{ASt1-3,St1-2,St1-1}$	≈890	≈813	≈260	
		1.2695	$ASt_{1-3}St_{2-1}$	**$\omega_{f1} - 2\omega_{SRS1} + \omega_{SRS3} = \omega_{ASt1-3,St2-1}$	≈890		≈260	
		1.2868	St_{2-2}	*$\omega_{f1} - 2\omega_{SRS2} = \omega_{St2-2}$		≈813		
		1.2997	$St_{1-2}St_{1-1}$	**$\omega_{f1} - \omega_{SRS1} - \omega_{SRS2} = \omega_{St1-2,St1-1}$	≈890	≈813		
		1.3128	St_{2-1}	*$\omega_{f1} - 2\omega_{SRS1} = \omega_{St2-1}$	≈890			
		1.3262	$ASt_{1-2}St_{3-1}$	**$\omega_{f1} - 3\omega_{SRS1} + \omega_{SRS2} = \omega_{ASt1-2,St3-1}$	≈890	≈813		
		1.3592	$St_{1-3}St_{2-1}$	**$\omega_{f1} - 2\omega_{SRS1} - \omega_{SRS3} = \omega_{St1-3,St2-1}$	≈890		≈260	
		1.4312	$ASt_{1-3}St_{3-1}$	**$\omega_{f1} - 3\omega_{SRS1} + \omega_{SRS3} = \omega_{ASt1-3,St3-1}$	≈890		≈260	
		1.4697	$St_{1-2}St_{2-1}$	**$\omega_{f1} - 2\omega_{SRS1} - \omega_{SRS2} = \omega_{St1-2,St2-1}$	≈890	≈813		
		1.4865	St_{3-1}	*$\omega_{f1} - 3\omega_{SRS1} = \omega_{St3-1}$	≈890			
		1.5463	$St_{1-3}St_{3-1}$	**$\omega_{f1} - 3\omega_{SRS1} - \omega_{SRS3} = \omega_{St1-3,St3-1}$	≈890		≈260	
		1.7132	St_{4-1}	*$\omega_{f1} - 4\omega_{SRS1} = \omega_{St4-1}$	≈890			
	~*a*(*bc*, *bc*)~a	0.4212	$\lambda_{s\text{-}SFG}$ (λ_{St1-1}, λ_{St2-1})	**$\omega_{St1-1} + 2\omega_{St2-1}$[e]	≈890			

Table 2 continued

Excitation condition		Nonlinear $\chi^{(3)}$- lasing components			SRS-promoting vibration modes, cm^{-1}			
λ_f, μm	Pumping condition[a]	Wavelength, μm[b]	Line[c]	Attribution of nonlinear generation[d]	ω_{SRS1}	ω_{SRS2}	ω_{SRS3}	ω_{SRS4}
	(see Fig. 6a)	0.4376	λ_{THG} ($\lambda_{St2\text{-}1}$)	$^{**}3\omega_{St2\text{-}1}$[e]	≈890			
	~$a(bc, bc)$~a	0.4060	$\lambda_{s\text{-}SFG}$ ($\lambda_{St1\text{-}1}$, $\lambda_{St2\text{-}1}$)	$^{**}2\omega_{St1\text{-}1} + \omega_{St2\text{-}1}$[e]	≈890			
	(see Fig. 6b)	0.4212	$\lambda_{s\text{-}SFG}$ ($\lambda_{St1\text{-}1}$, $\lambda_{St2\text{-}1}$)	$^{**}\omega_{St1\text{-}1} + 2\omega_{St2\text{-}1}$[e]	≈890			
	~$a(bc, bc)$~a	0.4376	λ_{THG} ($\lambda_{St2\text{-}1}$)	$^{**}3\omega_{St2\text{-}1}$[e]	≈890			
	(see Fig. 6c)	0.4060	$\lambda_{s\text{-}SFG}$ ($\lambda_{St1\text{-}1}$, $\lambda_{St2\text{-}1}$)	$^{**}2\omega_{St1\text{-}1} + \omega_{St2\text{-}1}$[e]	≈890			
		0.4212	$\lambda_{s\text{-}SFG}$ ($\lambda_{St1\text{-}1}$, $\lambda_{St2\text{-}1}$)	$^{**}\omega_{St1\text{-}1} + 2\omega_{St2\text{-}1}$[e]	≈890			
0.53207	$c(a, a)c$	0.5080	$ASt_{1\text{-}1}$	$^{*}\omega_{f2} + \omega_{SRS1} = \omega_{ASt1\text{-}1}$	≈890			
	(see Fig. 7)	0.53207	λ_{f2}	ω_{f2}				
		0.5561	$St_{1\text{-}2}$	$\omega_{f2} - \omega_{SRS2} = \omega_{St1\text{-}2}$		≈813		
		0.5585	$St_{1\text{-}1}$	$\omega_{f2} - \omega_{SRS1} = \omega_{St1\text{-}1}$	≈890			
		0.5871	$St_{1\text{-}2}St_{1\text{-}1}$	$^{**}\omega_{f2} - \omega_{SRS1} - \omega_{SRS2} = \omega_{St1\text{-}2,St1\text{-}1}$	≈890	≈813		
		0.5877	$St_{2\text{-}1}$	$^{*}\omega_{f2} - 2\omega_{SRS1} = \omega_{St2\text{-}1}$	≈890			
		0.6202	$St_{3\text{-}1}$	$^{*}\omega_{f2} - 3\omega_{SRS1} = \omega_{St3\text{-}1}$	≈890			

[a] Notations are used in analogy to [26]. The characters between parentheses are (from left to right): the polarization direction of the pump wave and the nonlinear laser generation, respectively, while the characters to the left and to right of the parentheses are the direction of the wave normals of the pump wave and of the generated nonlinear-laser components, respectively. In the case of $c(ab, ab)c$ the polarization direction for pump and $\chi^{(3)}$-lasing scattered emission was directed between the a and b axes

[b] Measurement accuracy is ±0.0003μm

[c] Notations used here: for example, the notation St1-2ASt1-1 (for the 0.9009 μm line) is defined as the first Stokes component (related to the second SRS-promoting vibration mode $\omega_{SRS2} \approx 813\ cm^{-1}$) generated from the first anti-Stokes emission (connected with the first SRS-active vibration mode $\omega_{SRS1} \approx 890\ cm^{-1}$)

[d] The single- and double-asterisk mark the cascaded and cross-cascaded SRS and RFWM $\chi^{(3)}$-lasing processes, respectively. They are designated by the simplified notations for SRS and RFWM cascaded and cross-cascaded ($\chi^{(3)} \leftrightarrow \chi^{(3)}$)-lasing processes. The full designations of these processes should be, for example for the SRS cascade of the Stokes lasing, $\omega_{f1} - 2\omega_{SRS3} = (\omega_{f1} - \omega_{SRS3} - \omega_{SRS3}) = \omega_{St2\text{-}3}$ for the line at 1.1265 μm. For the anti-Stokes lasing $\omega_{f1} + \omega_{SRS1} = \omega_{ASt1\text{-}1}$ at 0.9721 μm, the full designation including all four involved waves is $\omega_{f1} + \omega_{SRS1} = [\omega_{f1} + \omega_{f1} - (\omega_{f1} - \omega_{SRS1})] = [\omega_{f1} + \omega_{f1} - \omega_{St1\text{-}1})] = \omega_{ASt1\text{-}1}$

[e] Phase matching of the self-SFG and THG components at 0.4060 μm, 0.4212 μm and 0.4376 μm was obtained for angle tuning around the crystal b-axis of 14°, 20°, and 26°, respectively. The crystal a-axis references the position of 0° rotation

In addition, the pump beam wavelength can optionally be converted to λ_{f2} = 0.53207 μm by second harmonic generation (SHG) in a $KTiOPO_4$ (KTP) crystal with approximately 25 % efficiency. This results in a reduced pulse duration of 60 ps and a focus diameter of about 40 μm. A Schott BG39 filter glass (1 mm thickness) with a transmission of 0.015 % at 1.06415 μm and of 0.96 % at 0.53207 μm wavelength (see Fig. 1b) is inserted behind the KTP crystal to suppress the infrared component.

Different excitation geometries are adjusted by a customized sample stage with three translational and three rotational degrees of freedom. This provides alignment of the sample at any angle with respect to the pump beam direction and polarization. Due to the conical emission characteristics of Raman four-wave mixing and other nonlinear processes in the sample, it is necessary to exploit the complete acceptance angle of the grating spectrometer in Czerny–Turner arrangement used for signal detection (McPherson Model 270, 6.8 Å/pixel dispersion, 150 lines/mm grating). A spherical, bi-convex fused silica lens (L_2) with 50.8 mm diameter and 100 mm focal length, followed by a cylindrical plano-convex fused silica lens (L_3) with a size of 50 × 50 mm^2 and same focal length of 100 mm image the scattered radiation onto the variable spectrometer entrance slit. An additional lens can be inserted behind the sample for the detection of scattering components emitted in very large angles. Moreover, a BG39 glass filter can optionally be added in case of IR pumping in order to diminish the strong pump radiation incident on the detector. The spectral composition of the output radiation is finally detected by a Si-CCD line sensor (Hamamatsu S3924-1024Q) for measurements in the UV and visible spectral region, whereas an InGaAs-CMOS sensor is applied (Hamamatsu G9204-512D) for the detection of spectral components between 0.9 and 1.7 μm (see Fig. 1c).

2.1 SRS spectroscopy of $\chi^{(3)}$-nonlinear lasing

A selection of Raman-induced $\chi^{(3)}$-lasing spectra of a $Gd_{0.5}Lu_{0.5}VO_4$ crystal recorded in different excitation geometries are shown in Figs. 2, 3, 4, 5, 6. They clearly demonstrate its many-phonon high-order Stokes and anti-Stokes generation in the UV, visible and near-IR range, as well as single and few-stage cascaded and cross-cascaded self-SFG. Results of their analysis are summarized in Table 1. These results evidence that the bi-TR-cationic "mixed" $Gd_{0.5}Lu_{0.5}VO_4$ vanadate with a partially disordered tetragonal structure, as well as the four known SRS-active single-TR-cationic $TRVO_4$ crystals with the ordered D_{4h}^{19}-tetragonal structure exhibit many common nonlinear photon–phonon interactions (see Table 2 and its references).

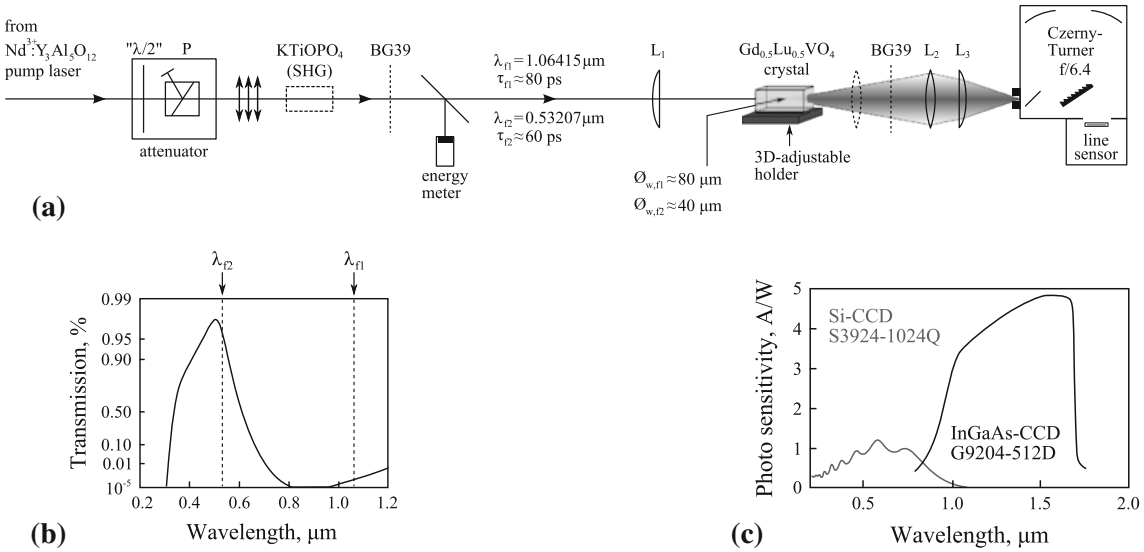

Fig. 1 **a** Schematic diagram of the registration part of experimental setup used for the SRS-spectroscopy of the $Gd_{0.5}Lu_{0.5}VO_4$ crystal (*P* polarizer, *L1–L3* lenses, see also text). **b** Transmission spectrum of the utilized BG39 glass filter (1 mm thickness, data taken from Schott datasheet). The fundamental wavelengths λ_{f1} = 1.06415 μm and λ_{f2} = 0.53207μm are indicated by *dashed lines*. **c** Spectral sensitivity of the employed Si- and InGaAs-CCD line sensors (data taken from Hamamatsu Photonics K.K. datasheet)

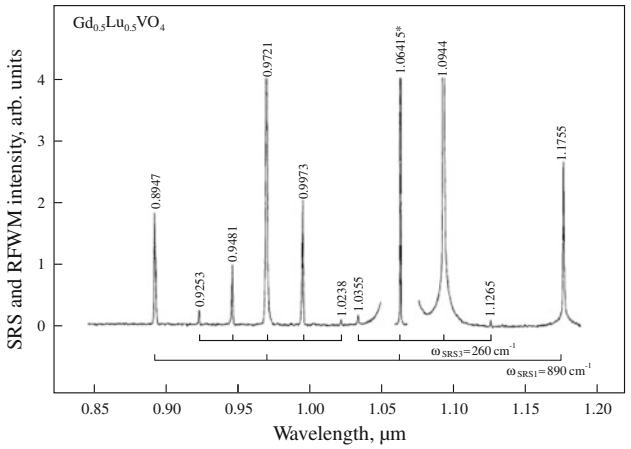

Fig. 2 Room-temperature SRS and RFWM spectrum of tetragonal $Gd_{0.5}Lu_{0.5}VO_4$ recorded in excitation geometry *c*(*a*,*a*)*c* with picosecond pumping at λ_{f1} = 1.06415 μm wavelength. The wavelengths of all lines (pump line is *asterisked*) are given in μm, their spectral intensities are shown without correction for the spectral sensitivity of the used analyzing system including the Si-CCD line sensor (see Fig. 1c). The spacings of the Stokes and anti-Stokes lasing components resulting from the two SRS-promoting vibration modes $\omega_{SRS1} \approx$ 890 cm^{-1} and $\omega_{SRS3} \approx$ 260 cm^{-1} and are indicated by the *horizontal scale brackets*

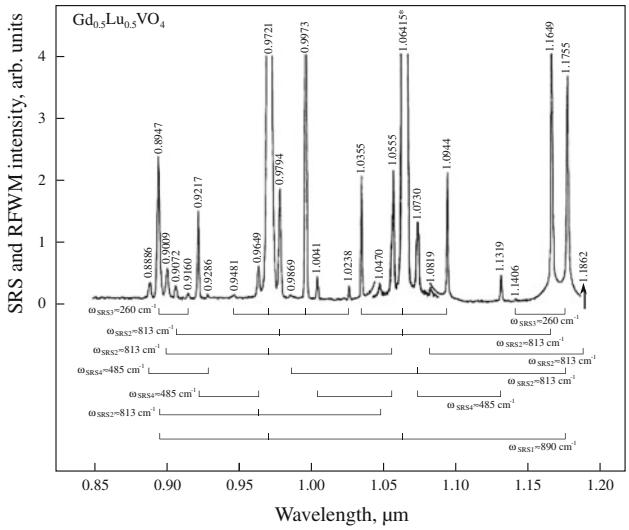

Fig. 3 Room-temperature SRS and RFWM spectrum of tetragonal $Gd_{0.5}Lu_{0.5}VO_4$ recorded in excitation geometry *c*(*ab*,*ab*)c with picosecond pumping at λ_{f1} = 1.06415 μm wavelength. The spacings of the Stokes and anti-Stokes lasing components resulting from the four SRS-promoting vibration modes $\omega_{SRS1} \approx$ 890 cm^{-1}, $\omega_{SRS2} \approx$ 813 cm^{-1}, $\omega_{SRS3} \approx$ 260 cm^{-1} and $\omega_{SRS4} \approx$ 485 cm^{-1} are indicated by the *horizontal scale brackets*. The *arrow* indicates the position of the line $\lambda_{ASt1\text{-}2,St2\text{-}1}$ (at 1.1862 μm wavelength) which is not recorded in this measurement with the Si-CCD sensor. Other used notations as in Fig. 2

Picosecond pumping at λ_{f1} = 1.06415 μm wavelength of the studied vanadate yielded a more than sesquioctave (≈11,570 cm^{-1}) wide SRS frequency comb (see Figs. 3, 4) spanning from fourth Stokes sideband at $\lambda_{St4\text{-}1}$ = 1.7132 μm ($\omega_{St4\text{-}1}$ = 5,837 cm^{-1}) to the ninth anti-Stokes sideband at $\lambda_{ASt9\text{-}1}$ = 0.5745 μm ($\omega_{ASt9\text{-}1}$ = 17406 cm^{-1}).

In addition, several $\chi^{(3)}$-cross-cascaded lasing processes occur under participation of two different SRS-promoting vibration modes (ω_{SRS1} and ω_{SRS2}, ω_{SRS1} and ω_{SRS3} as well as ω_{SRS2} and ω_{SRS4}).

Moreover, this crystal exhibits complex $\chi^{(3)}$-cross-cascaded lasing processes (see Figs. 3, 4, 5; Table 1) involving three different SRS-modes (ω_{SRS1}, ω_{SRS2} and ω_{SRS4}, as well

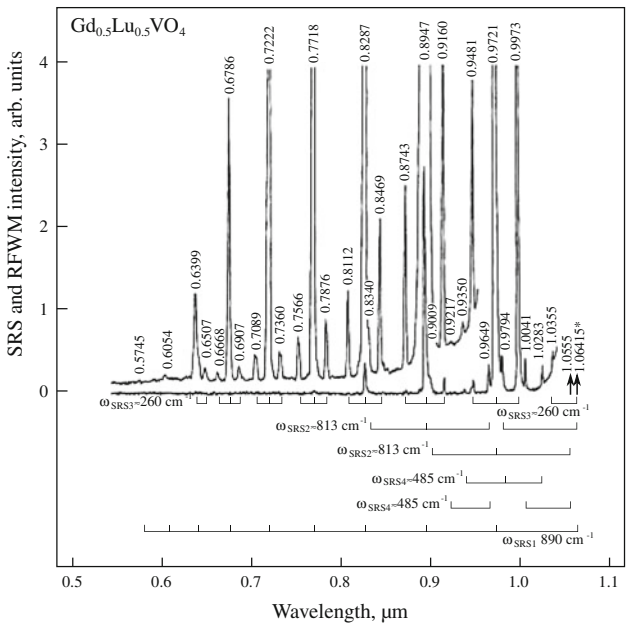

Fig. 4 Room-temperature SRS and RFWM spectra of tetragonal $Gd_{0.5}Lu_{0.5}VO_4$ recorded in excitation geometry *c*(*ab*,*ab*)c with picosecond pumping (two power levels) at λ_{f1} = 1.06415 μm wavelength. The *arrows* indicate the positions of pump line at 1.06415 μm wavelength and the line $\lambda_{St1\text{-}2,ASt1\text{-}1}$ (at 1.0555 μm) whose intensities are much higher than the intensities of other lines in the shown spectrum. Other used notations as in Figs. 2 and 3

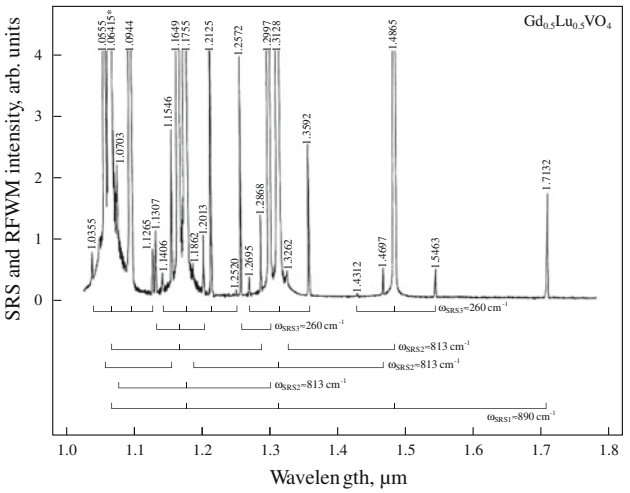

Fig. 5 Room-temperature SRS and RFWM spectrum of tetragonal $Gd_{0.5}Lu_{0.5}VO_4$ recorded in excitation geometry *c*(*ab*,*ab*)*c* with picosecond pumping at λ_{f1} = 1.06415 μm wavelength. The wavelengths of all lines (pump line is *asterisked*) are given in μm, their spectral intensities are shown without correction for the spectral sensitivity of the used analyzing system including the InGaAs line sensor (see Fig. 1c). The spacings of the Stokes and anti-Stokes lasing components resulting from the three SRS-promoting vibration modes $\omega_{SRS1} \approx 890$ cm^{-1}, $\omega_{SRS2} \approx 813$ cm^{-1} and $\omega_{SRS3} \approx 260$ cm^{-1} are indicated by the *horizontal scale brackets*. Other used notations as in Fig. 2

as ω_{SRS1}, ω_{SRS2} and ω_{SRS3}). The conducted experiments additionally revealed a peculiarity of the many-mode cross-cascade generation which requires a serious comprehension.

Fig. 6 Room-temperature spectra of tetragonal $Gd_{0.5}Lu_{0.5}VO_4$ recorded in excitation geometry $\sim a(bc, bc) \sim a$ with picosecond pumping at λ_{f1} = 1.06415 μm wavelength showing phase matched generation of self-SFG and THG at 0.4060 μm, 0.4212 μm and 0.4376 μm, respectively. Rotation of the crystal around the *b*-axis by 14°, 20°, and 26° with respect to the crystal *a*-axis allowed tuning the phase matching conditions

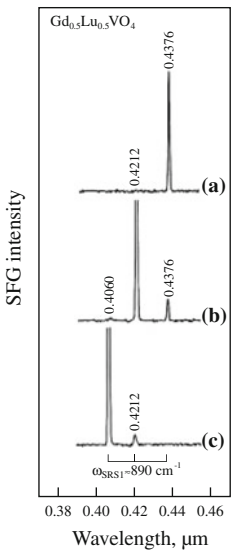

In all recorded spectra the SRS-mode $\omega_{SRS4} \approx 485$ cm^{-1} always manifested itself only in conjunction with the mode $\omega_{SRS3} \approx 813$ cm^{-1} in both the two and the three cross-cascaded processes.

Within the framework of our $\chi^{(3)}$-lasing measurements, we were able to roughly estimate the steady-state (s-s) Raman gain coefficient (g_{ssR}) of the $Gd_{0.5}Lu_{0.5}VO_4$ crystal for its first Stokes generation at $\lambda_{St1\text{-}1}$ = 1.1755 μm wavelength which is related to its SRS-promoting vibration mode $\omega_{SRS1} \approx 890$ cm^{-1}. This procedure is possible since our pumping pulse duration ($\tau_{f1} \approx 80$ ps) well satisfies the necessary condition $\tau_{f1} \gg T_2 = (\pi \Delta \nu_{R1})^{-1} \approx 2$ ps (where T_2 and $\nu_{R1} \approx 5$ cm^{-1} denote the phonon dephasing time of the SRS-promoting vibration transition and the linewidth of its Raman shifted line in the spontaneous Raman scattering spectrum (see Fig. 8), respectively). The determination of the gain coefficient based on the well known relation [27, 28] $g_{ssR} \cdot I_f^{thr} \cdot l_{SRS} \approx 30$ was realized by comparison of the threshold pump intensity (I_f^{thr}) that has to be applied for a reliable detection of the first-Stokes lasing signal of the title crystal on the one hand and of a reference crystal on the other hand. For this purpose, a $GdVO_4$ crystal of similar SRS-active length $l_{SRS} = 25$ mm was used as a reference sample with a known gain coefficient value of $g_{ssR}^{St1\text{-}1} \geq 4.5$ cm GW^{-1} for its first Stokes lasing at 1.1744 μm wavelength [7]. The performed measurement yielded a slightly lower (factor 0.95) threshold for the first Stokes lasing at $\lambda_{St1\text{-}1}$ = 1.1755 μm wavelength for the "mixed" vanadate $Gd_{0.5}Lu_{0.5}VO_4$ compared to the threshold for the first-Stokes lasing at $\lambda_{St1\text{-}1}$ = 1.1744 μm wavelength in $GdVO_4$. Taking the shorter sample length of the $Gd_{0.5}Lu_{0.5}VO_4$ crystal ($l_{SRS} = 22.4$ mm) into account, this leads to a comparably higher steady-state Raman gain coefficient for the title crystal of about $g_{ssR}^{St1\text{-}1} \geq 5.3$ cm GW^{-1}. However, it should be noted that the sensitivity

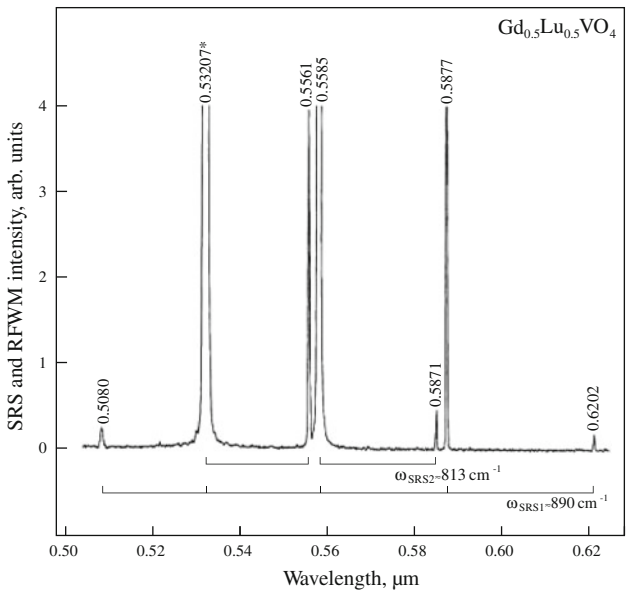

Fig. 7 Room-temperature SRS and RFWM spectrum of tetragonal $Gd_{0.5}Lu_{0.5}VO_4$ recorded in excitation geometry $c(a,a)c$ with picosecond pumping at λ_{f2} = 0.53207 μm wavelength. Used notations as in Fig. 2

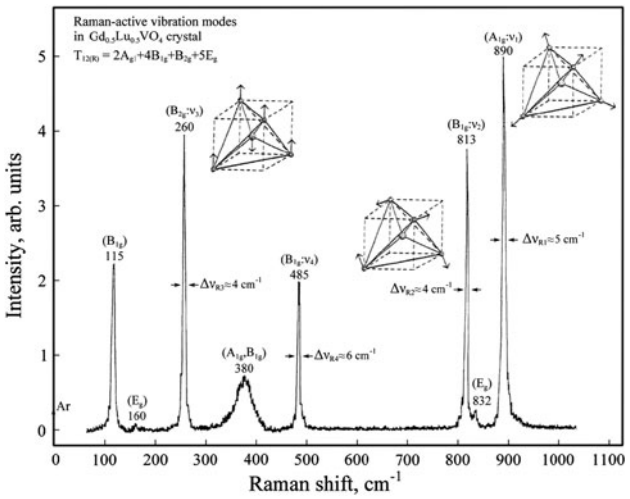

Fig. 8 Room-temperature polarized spontaneous Raman scattering spectrum of the tetragonal $Gd_{0.5}Lu_{0.5}VO_4$ single crystal under Ar-ion laser excitation at 0.488 μm wavelength (shown by the *arrow*). The Raman-shifted lines are given in cm^{-1} with an indication of the vibration mode symmetry (*in parentheses*). The FWHM linewidths are only indicated for the lines related to SRS-promoting internal vibration modes of the crystal recorded in the present work. The *insets* show the atomic displacements of the tetrahedral $(VO_4)^{3-}$-ionic groups for three SRS-active modes

of the detector used for the determination of the $GdVO_4$ gain coefficient in [7] was lower than in the experiments presented here which explains the lower threshold energy and, in turn, the higher gain coefficient value for the title crystal.

From the results of the present experiments on $\chi^{(3)}$-nonlinear lasing processes in $Gd_{0.5}Lu_{0.5}VO_4$ it follows that it exhibits four SRS-active vibration modes, which can simultaneously manifest in high-order spectra of its Stokes and anti-Stokes generation (see Figs. 3, 4). Now, we briefly discuss their vibration nature. The primitive cell (with $Z = 2$) of the $Gd_{0.5}Lu_{0.5}VO_4$ crystal (as well as other D_{4h}^{19}-tetragonal zircon-type structure $TRVO_4$ vanadates) comprises 12 atoms (Gd and Lu are treated as a single atom) giving rise to $3NZ = 36$ degrees of vibration freedom described by the D_{4h}-irreducible representations (at $\mathbf{k} = 0$) as $\Gamma_{36} = 2A_{1g} + 4B_{1g} + B_{2g} + 5E_g + A_{2g} + B_{1u} + A_{1u} + 2B_{2u} + 4A_{2u} + 5E_u$ (see e.g., [29]). Among them, the first four species ($2A_{1g} + 4B_{1g} + B_{2g} + 5E_g$) are modes that should appear in the spontaneous Raman scattering spectrum (see e.g., [30–33]). Part of these ($2A_{1g} + 2B_{1g} + B_{2g} + 2E_g$) relate to the internal vibrations of the tetrahedral $(VO_4)^{3-}$ units. Figure 8 shows the polarized Raman spectrum of the title crystal recorded in roughly the same excitation geometry $\approx c(ab,ab)\approx c$, which was used to obtain the spectrum presented in Fig. 3 with all four registered SRS-active vibration modes. The analysis showed that they all belong to the internal optical modes of the tetrahedral $(VO_4)^{3-}$-ionic groups (see insets in Fig. 8), in particular, the most active ones: $\omega_{SRS1} \approx 890\ cm^{-1}$ related to the totally symmetric (stretching) $A_{1g}(\nu_1)$ vibrations, the $\omega_{SRS2} \approx 813\ cm^{-1}$ mode to $B_{1g}(\nu_3)$, the $\omega_{SRS3} \approx 260\ cm^{-1}$ mode to $B_{2g}(\nu_2)$, and the $\omega_{SRS4} \approx 485\ cm^{-1}$ mode to $B_{1g}(\nu_4)$. Here, we must note that the manifestation of Stokes and anti-Stokes generation associated with the ω_{SRS4} mode was observed only in conjunction with the appearance of the $\chi^{(3)}$-lasing components related to the ω_{SRS2} mode. This is an interesting feature of the investigated $\chi^{(3)}$-cross-cascaded lasing in the $Gd_{0.5}Lu_{0.5}VO_4$ crystal and requires further study.

2.2 Conclusion

The research carried out concerning "mixed" vanadate $Gd_{0.5}Lu_{0.5}VO_4$ exhibiting a partially disordered structure enriched our knowledge on $\chi^{(3)}$-nonlinear-laser phenomena in tetragonal $TRVO_4$ crystals with zircon-type structure. Many of them are known as excellent host-crystals for Ln^{3+}-lasants and birefringent materials. We discovered various manifestations of photon–phonon interactions in $Gd_{0.5}Lu_{0.5}VO_4$ related to its cubic $\chi^{(3)}$-nonlinearity, namely efficient Stokes (4 sidebands) and anti-Stokes (9 sidebands) generation leading to a more than sesqui-octave wide ($\approx$11,570 cm^{-1}) lasing comb (see Table 1); four SRS-promoting modes that belong to internal vibrations of the tetrahedral $(VO_4)^{3-}$ units; cascaded and cross-cascaded $\chi^{(3)} \leftrightarrow \chi^{(3)}$ many-phonon generation as well as up-conversion

Table 3 Steady-state first Stokes Raman gain coefficients for the known SRS-active $TRVO_4$ vanadates as well as for some widely used commercial SRS-active tungstates, the latter were taken from [2]

Crystal	Room-temperature $\chi^{(3)}$ first-Stokes lasing		
	λ_{St1} (μm)[a]	$g_{ssR}^{St_1}$ (cm·GW^{-1})	ω_{SRS} (cm^{-1})[b]
YVO_4	1.1755	≥4.5	≈890
$GdVO_4$	1.1744	≥4.5	≈882
$YbVO_4$	1.1765	≥2.9	≈897
$LuVO_4$	1.1769	≥3.2	≈900
$Gd_{0.5}Lu_{0.5}VO_4$	1.1755	≥5.3	≈890
α-$KY(WO_4)_2$	1.1776	≥3.6	≈905
α-$KGd(WO_4)_2$	1.1589	≥4.4	≈768
$PbWO_4$	1.1770	≥3.1	≈901

[a] With picosecond pumping at 1.06415 μm

[b] Related to SRS-promoting vibration mode

$\chi^{(3)}$-self-SFG interactions. We estimated the steady-state first-Stokes Raman gain coefficient to ≥ 5.3 cm/GW. Table 3 lists analogous coefficients for known SRS-active isostructural $TRVO_4$ vanadates, as well as for some widely used commercial SRS-active tungstates, the latter taken from [2].

By this research we have demonstrated the attractive $\chi^{(3)}$-nonlinear potential of the tetragonal $Gd_{0.5}Lu_{0.5}VO_4$ crystal with regard to Raman laser converters in the visible and near-IR spectral range. We believe that this vanadate—when doped with Ln^{3+}-ions (e.g., Nd^{3+} and Yb^{3+})—is promising for the development of self-Raman lasers. We intend that this work as well as our previous publications on SRS spectroscopy of $TRVO_4$ vanadates can stimulate other researchers to search for new $\chi^{(3)}$-active crystals with D_{4h}^{19}-tetragonal zircon-type structure, including also, for example $TRPO_4$ phosphates (one of them, YPO_4, has been studied recently [34]).

Acknowledgments The authors wish to note that the investigations were considerably promoted through mutual scientific help within the "Joint Open Laboratory for Laser Crystals and Precise Laser Systems", and were stimulated by research programs of the Institute of Crystallography of the Russian Academy of Sciences, by the Institute of Optics and Atomic Physics of the Technical University of Berlin, by the Institute for Laser Science of the University of Electro-Communications. One of us (A.A.K) is grateful also to the Fundamental Program "Extreme Light Fields and Their Applications" of the Presidium of Russian Academy of Sciences, to the Russian Foundation for Basic Research, and to the Alexander von Humboldt Foundation.

References

1. M.J. Weber, *Handbook of Laser Wavelengths*. (CRC Press, Boca Raton, FL, 2000)
2. A.A. Kaminskii, Laser Photon Rev. **1**, 93 (2007)
3. J.R. O'Conner, Appl. Phys. Lett **9**, 407 (1966)
4. J.J. Rubin, L.G. Van Uitert, J. Appl. Phys. **37**, 2920 (1966)
5. A.A. Kaminskii, G.A. Bogomolova, L. Li, Inorg. Mater. (USSR) **5**, 673 (1969)
6. E.A. Maunders, L.G. DeShazer, J. Opt. Soc. Am. **66**, 1405 (1976)
7. A.A. Kaminskii, K. Ueda, H.J. Eichler, Y. Kuwano, H. Kouta, S.N. Bagaev, T.H. Chiba, J.C. Barnes, G.M.A. Gad, T. Murai, J. Lu, Opt. Commun. **194**, 201 (2001)
8. A.A. Kaminskii, *Laser Crystal, Their Physics and Properties* (Springer, Berlin, 1980 and 1990)
9. A.A. Kaminskii, *Crystalline Lasers: Physical Processes and Operating Schemes* (CRC Press, Boca Raton, Fl, 1996)
10. A.A. Kaminskii, Sov. Phys. JETP **31**, 216 (1970)
11. A.A. Kaminskii, K. Ueda, H.J. Eichler, Y. Kuwano, H. Kouta, S.N. Bagayev, T.H. Chiba, J.C. Barnes, J. Lu, Laser Phys. **11**, 1124 (2001)
12. Y.F. Chen, Opt. Lett. **29**, 1915 (2004)
13. Y.F. Chen, Opt. Lett. **29**, 2172 (2004)
14. V.E. Kisel, A.E. Troshkin, N.A. Tolstik, V.G. Shcherbitsky, N.V. Kultshov, V.M. Matrosov, T.A. Matrosova, M.I. Kupchenko, Appl. Phys. B **80**, 471 (2005)
15. T.T. Basiev, S.V. Vassilliev, V.A. Konjushkin, V.V. Osiko, A.I. Zagumennyi, V.D. Zavartsev, S.A. Kutavoi, I.A. Shcherbakov, Laser Phys. Lett. **1**, 237 (2004)
16. Y.F. Chen, Opt. Lett. **29**, 2632 (2004)
17. A.A. Kaminskii, H.J. Eichler, H. Rhee, K. Ueda, K. Oka, H. Shibata, Laser Phys. **18**, 1546 (2008)
18. A.A. Kaminskii, H. Rhee, H.J. Eichler, K. Ueda, K. Oka, H. Shibata, Appl. Phys. B **93**, 865 (2008)
19. A.A. Kaminskii, B. Bettinelli, J. Dong, D. Jaque, K. Ueda, Laser Phys. Lett. **6**, 374 (2009)
20. Y.F. Chen, M.L. Ku, L.Y. Trai, Y.C. Chen, Opt. Lett. **29**, 2279 (2004)
21. Y.T. Chang, H.L. Chang, K.W. Su, Y.F. Chen, Opt. Express **17**, 11892 (2009)
22. T. Omtsu, A. Lee, H.M. Pask, J. Piper, Appl. Phys. B **97**, 799 (2009)
23. Y.F. Lu, W.B. Cheng, Z. Xong, J. Lu, L.J. Xu, G.C. Sun, Z.M. Zhau, Laser Phys. Lett. **7**, 787 (2010)
24. Y.V. Duan, G. Zhang, Y.J. Jang, Q.L. Jin, H.Y. Wang, H.Y. Zhu, Laser Phys. **21**, 1859 (2011)
25. A.A. Kaminskii, Sov. Phys. JETP **24**, 33 (1967)
26. T.C. Damen, S.P.S. Porto, B. Tell, Phys. Rev. **142**, 570 (1966)
27. W. Kaiser, M. Maier, in *Laser Handbook*, vol. 2, ed. by F.T. Arecchi, E.O. Schulz-Dubois (North-Holland, Amsterdam, 1972), p. 1077
28. Y.R. Shen, *The Principles of Nonlinear Optics* (Wiley, New York, 1984)
29. D.L. Rouseau, R.P. Bauman, S.P.S. Porto, J. Raman Spectrosc. **10**, 253 (1981)
30. S.A. Muller, H.H. Caspers, H.E. Rast, Phys. Rev. **168**, 964 (1966)
31. A. Chaves, S.P.S. Porto, Solid State Commun. **10**, 1075 (1972)
32. S.J. Duclos, A. Jayarama, G.P. Espinosa, A.S. Cooper, R.G. Maines, J. Phys. Chem. Sol. **50**, 769 (1989)
33. C.C. Santos, I. Guedes, C.-.K. Loong, L.A. Boater, Vib. Spectrosc. **45**, 95 (2007)
34. A.A. Kaminskii, M. Bettinelli, A. Speghini, H. Rhee, H.J. Eichler, G. Marriotto, Laser Phys. Lett. **5**, 367 (2008)